scientific reports

OPEN

Design, synthesis, and investigation of novel 5-arylpyrazole-glucose hybrids as α-glucosidase inhibitors

Roshanak Hariri[1], Mina Saeedi[2,3], Somayeh Mojtabavi[4], Simin Alizadeh[5], Ahmad Ebadi[5], Mohammad Ali Faramarzi[4], Mohsen Amini[1], Mohammad Sharifzadeh[6], Mahmood Biglar[1] & Tahmineh Akbarzadeh[1,3]✉

Considering the global incidence of diabetes, developing new compounds to lower blood sugar levels has become increasingly crucial. As a result, there has been a growing focus on the synthesis of α-glucosidase inhibitors in recent years. This study investigated design, synthesis, and effects of novel 5-aryl pyrazole-glucose hybrids as α-glucosidase inhibitors. Thirteen derivatives from this class of compounds were synthesized, demonstrating superior in vitro inhibitory effects (IC_{50} values ranging from 0.5 to 438.6 μM, compared to acarbose at 750.0 μM). Among them, compound 8g (IC_{50} = 0.5 μM) was selected for further investigations and the kinetic studies revealed that it is a competitive inhibitor (K_i = 0.46 μM). Fluorescence assays indicated changes in the fluorescence intensity, while thermodynamic analyses suggested that compound 8g promoted a transition of the enzyme into an unfolded state. Furthermore, in vivo studies demonstrated that 8g effectively reduced blood sugar levels in rats at doses comparable to acarbose. Molecular docking studies revealed that this compound interacted with the enzyme's active site, and molecular dynamics simulations showed that pharmacophores engaged in various interactions with the enzyme.

Keywords Arylpyrazole, Glucose, Alpha-glucosidase, Inhibitory effects, Synthesis

Diabetes is one of the most significant chronic diseases in the world with a high incidence of 536.6 million cases in 2021 which is predicted to rise to 783.2 million by 2045[1]. Diabetes leads to retinopathy, nephropathy, neuropathy, and cardiovascular disease[2–4]. Type 1 and type 2 diabetes are distinguished by the body's inability to make insulin in the former and its improper use in the latter. The disease can be treated with medications such as biguanides, agonists of peroxisome proliferator-activated receptor-γ, sulfonylureas, and α-glucosidase inhibitors[5–7].

α-Glucosidase is an enzyme found in the brush border of the intestine that facilitates the breakdown of polysaccharides and disaccharides into absorbable glucose[8]. The regulation of postprandial blood glucose occurs through inhibiting this enzyme, and its inhibitors effectively manage blood sugar levels[9].

α-Glucosidase inhibitors competitively block the enzyme, hindering carbohydrate hydrolysis and resulting in delayed glucose absorption in the small intestine. This mechanism helps regulate postprandial blood sugar levels and plays a crucial role in managing postprandial hyperglycemia. This approach is part of contemporary therapeutic strategies aimed at stabilizing blood glucose levels in diabetic patients, particularly those with type 2 diabetes. Research indicates that, since α-glucosidase significantly influences carbohydrate metabolism, inhibiting this enzyme in the gastrointestinal tract is one of the most effective methods for lowering glucose levels and improving control over type 2 diabetes. Consequently, scientists are currently focused on developing α-glucosidase inhibitors[8,10,11].

[1]Department of Medicinal Chemistry, Faculty of Pharmacy, Tehran University of Medical Sciences, Tehran, Iran. [2]Medicinal Plants Research Center, Faculty of Pharmacy, Tehran University of Medical Sciences, Tehran, Iran. [3]Persian Medicine and Pharmacy Research Center, Tehran University of Medical Sciences, Tehran, Iran. [4]Department of Pharmaceutical Biotechnology, Faculty of Pharmacy, Tehran University of Medical Sciences, Tehran, Iran. [5]Department of Medicinal Chemistry, School of Pharmacy, Hamadan University of Medical Sciences, Hamadan, Iran. [6]Department of Pharmacology, Faculty of Pharmacy, Tehran University of Medical Sciences, Tehran, Iran. ✉email: akbarzad@tums.ac.ir

There are three drugs in the pharmaceutical market containing sugar moiety: acarbose, miglitol and voglibose. Depending on the patient's condition, these medications may be administered alone or in combination with other blood-glucose-lowering therapies. Furthermore, α-glucosidase inhibitors can lower hemoglobin A1c levels[9,12].

Due to the way these medications work, gastrointestinal problems including bloating, diarrhea, and abdominal pain are typically among their side effects[12]. Therefore, much research has recently been conducted to find new α-glucosidase inhibitors to develop molecules with greater efficacy and fewer side effects[13–15].

Among the structures that have been investigated, molecules with heterocyclic rings are particularly significant[16–18]. In this context, derivatives of 1,2,3-triazole[19], oxadiazole[20], imidazole[21], isatin[22], pyrazole[23], and other heterocycles have been reported. Among these compounds, pyrazole is the most significant heterocycle and studies have indicated that its derivatives can effectively inhibit α-glucosidase[23]. For instance, compounds **A**-**E** exemplify this category (Fig. 1)[24–28].

The in silico analysis demonstrated the specificity of compound **A** (*3,4-dimethylpyrano[2,3-c]pyrazol-6(1H)-one*), highlighting differences in binding energy and the number of bonds when interacting with α-glucosidase. Furthermore, cytotoxicity and hemolytic tests indicated that compound **A** has potential as a safe and specific treatment for postprandial hyperglycemia[24].

In the case of compound **B** (*N'-((3-(4-nitrophenyl)−1-phenyl-1H-pyrazol-4-yl)methylene)benzofuran-2-carbohydrazide*), the pyrazole group engages with Glu276 through a π-anion bond, and cytotoxicity assessments confirmed that this compound is non-toxic to normal cell lines[25].

Molecular docking analyses showed that various interactions securely bind compound **C** (*N'-(4-chlorobenzylidene)−5-phenyl-1H-pyrazole-3-carbohydrazide*) to the active site, which may account for its superior antidiabetic effects compared to the reference drug acarbose[26].

Additionally, preliminary pharmacokinetic evaluations of **D** (*3-(((4-(3-nitrophenyl)−1-phenyl-1H-pyrazol-3-yl)methylene)hydrazono)indolin-2-one*) revealed an intestinal absorption rate exceeding 97%, suggesting strong oral bioavailability. This compound also demonstrated low permeability across the blood-brain barrier, indicating a reduced likelihood of neurotoxicity. These findings imply that **D**, which exhibited activity against α-glucosidase in vitro, has the potential to serve as an orally active anti-diabetic agent[27].

The structure-activity relationship within category **E** (*N'-((3-(4-bromophenyl)−1-phenyl-1H-pyrazol-4-yl)methylene)−2-(2-(4-chlorophenyl)−4-oxoquinazolin-3(4H)-yl)acetohydrazide*) indicated that different substitutions on the aryl rings of the diphenyl pyrazole moiety influenced variations in inhibitory activity among the compounds. Kinetic studies of compound **E** showed that it inhibits α-glucosidase through a competitive mechanism, also molecular docking revealing that the pyrazole moiety is crucial for this interaction[28].
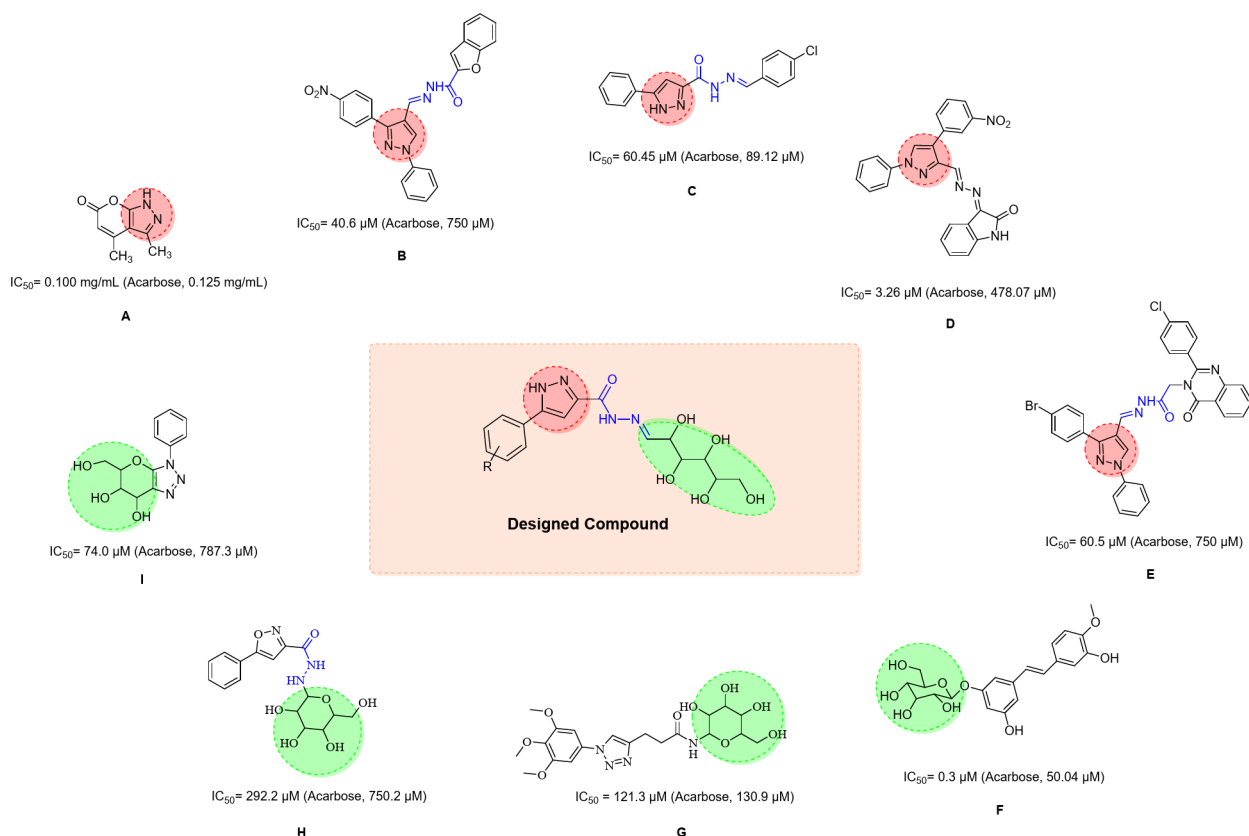
Fig. 1. α-Glucosidase inhibitors reported in the literature.

Due to their high solubility and low toxicity, carbohydrates are invaluable in drug discovery. Furthermore, they enhance the flexibility of the molecules to which they are attached[29]. Recent advancements in glycochemistry have sparked renewed interest in exploring carbohydrates within the field of medicinal chemistry[30].

On the other hand, the mechanism of action of α-glucosidase and the carbohydrate structures of drugs available on the market confirm that carbohydrates can play a significant role in inhibiting this enzyme[12,31]. The structures **F–I** in Fig. 1 are examples of compounds synthesized in recent years that have shown remarkable effects in inhibiting α-glucosidase. Studies indicate that compound **F** (*2-(3-hydroxy-5-((E)−3-hydroxy-4-methoxystyryl) phenoxy)−6-(hydroxymethyl)tetrahydro-2H-pyran-3,4,5-triol*) is metabolized and distributed, rapidly. Additionally, its bioavailability is very low, and it shows no toxic effects[32]. Moreover, docking studies suggest that the hydroxyl groups in the carbohydrate moiety of compounds **G** (*N-(3,4,5-trihydroxy-6-(hydroxymethyl) tetrahydro-2H-pyran-2-yl)−3-(1-(3,4,5-trimethoxyphenyl)−1H-1,2,3-triazol-4-yl)propanamide*) and **H** (*5-phenyl-N'-(3,4,5-trihydroxy-6-(hydroxymethyl)tetrahydro-2H-pyran-2-yl)isoxazole-3-carbohydrazide*) form hydrogen bonding interactions with the enzyme's active site, leading to a competitive inhibition[33,34]. Furthermore, experimental results indicated that compound **I** (*5-(hydroxymethyl)−3-phenyl-3,5,6,7-tetrahydropyrano[2,3-d] [1,2,3]triazole-6,7-diol*) inhibits α-glucosidase through hydrophobic, π-π stacking, and hydrogen bonding interactions[35].

It has been revealed that hybridization is an efficient method for obtaining new compounds with better efficacy. In particular, constructing hybrids containing carbohydrate scaffolds can improve the absorption, metabolism, distribution, excretion, and bioactivity of compounds. Additionally, combining different structures can synergize the desired effects. Therefore, hybridization is one of the most widely used methods in new drug discovery[27,30,36]. Furthermore, research has shown that the hydrazide moiety in the structure can interact with the active site of α-glucosidase resulting in the inhibition of the enzyme (**B, C, E, H**, Fig. 1)[25,26,34,37–39].

In this study, hybrids of two effective scaffolds—pyrazole and carbohydrate—connected by a hydrazide linker was designed and synthesized to provide potent α-glucosidase inhibitors.

Materials and methods

All the compounds and solvents used were obtained from Merck and Aldrich. The melting points of the synthesized compounds were determined on a Kofler hot stage apparatus. ^{1}H and ^{13}C NMR spectra were recorded on a Bruker FT-500 in DMSO-d_6 with TMS as an internal standard. IR spectra were obtained on a Nicolet Magna FTIR 550 spectrophotometer using KBr disks. Elemental analysis was performed using an Elementar Analysen system in the GmbH VarioEL CHNS mode.

Chemistry

General procedure for the synthesis of Ethyl 2,4-dioxo-4-aryl butanoate derivatives 3
First, 1.15 g sodium reacted with 13 mL dry ethanol to form sodium ethoxide. Subsequently, 125 mmol diethyl oxalate[1] was added dropwise to the sodium ethoxide generated in situ. The mixture was then stirred for one hour in an ice bath before the required amounts of acetophenone (**2**, 50 mmol) was added dropwise to the ethanol solution. After stirring the mixture for 24 to 48 h at room temperature and using a 5% sulfuric acid solution to adjust the pH to 2, the mixture was tested via thin layer chromatography (ethyl acetate/n-hexane: 1/10). The crude material was then extracted using brine, water, saturated sodium bicarbonate solution, and chloroform, in that order. After the organic phase was dried over anhydrous sodium sulfate, the solvent was removed under vacuum. After obtaining compound **3** as an oily result, it was utilized directly in the next stage without any further purification (yield: 70%)[40].

General procedure for the synthesis of Ethyl 5-arylpyrazole-3-carboxylate derivatives 5
A mixture of hydrazine hydrate (**4**, 3 mmol) and ethyl 2,4-dioxo-4-arylbutanoate derivative **3** (1 mmol) in ethanol (15 mL) was refluxed for 3 h. Following thin layer chromatography verification of the reaction's completion (ethyl acetate/n-hexane: 1/1.5), the reaction mixture was extracted with dichloromethane, a 4% sodium hydroxide solution, and brine, in that order. The solvent was finally removed via vacuum to produce ethyl 5- arylpyrazole−3-carboxylates **5** (yield: 89%)[41].

General procedure for the synthesis of 5-arylpyrazole-3-carbohydrazide derivatives 6
A mixture of hydrazine hydrate (**4**, 3 mmol) and ethyl 5-arylpyrazole-3-carboxylate derivative (**5**, 1 mmol) in ethanol (15 mL) was stirred at room temperature for 24–48 h. Compound **6** was finally obtained by adding ice and water to quench the reaction, filtering the precipitates, and then washing the mixture with water (yield: 92%)[42].

General procedure for the synthesis of compounds 8a-m
A mixture of compound **6** (1 mmol) and glucose (**7**, 1 mmol) in the presence of a catalytic amount of acetic acid was refluxed for 24 h (the reaction progress was monitored using thin layer chromatography). Next, the precipitates were filtered off and recrystallized from ethanol (yield: 40–65%)[34,43].

N'-(2,3,4,5,6-Pentahydroxyhexylidene)−5-phenyl-1H-pyrazole-3-carbohydrazide (**8a**).
White precipitates, Yield: 74%, mp 206–210 °C. IR (KBr, cm^{-1}): 3380, 2912, 1651, 1268. ^{1}HNMR (500 MHz, DMSO-d_6) (different isomers): 13.69 (s, 1H, NH), 9.69 (bs, 1H, NHCO), 7.88–7.66 (m, 3 H, CH=N, H2, H6), 7.46–7.14 (m, 4 H, H3, H4, H5, pyrazole), 5.97–5.89 (m, 1H, OH), 5.61–5.43 (m, 1H, OH), 5.10–4.88 (m, 3 H, 3 × OH), 4.54–4.21 (m, 2 H, 2 × CH of Carbohydrate), 3.90–3.89 (m, 1H, CH of Carbohydrate), 3.71–3.60 (m, 1H, CH of Carbohydrate), 3.54–3.46 (m, 1H, CH of Carbohydrate), 3.25–3.22 (m, 1H, CH of Carbohydrate), 3.17–3.14 (m, 1H, CH of Carbohydrate), 3.07–2.99 (m, 1H, CH of Carbohydrate) ppm. ^{13}CNMR (125 MHz, DMSO-d_6) (different isomers): 161.6, 159.1, 156.7, 147.7, 130.0, 129.4, 129.1, 125.7, 103.3, 91.2, 88.5, 78.5, 77.1,

74.1, 72.4, 71.5, 70.8, 64.1, 61.8 ppm. Calcd for $C_{16}H_{20}N_4O_6$: C, 52.74; H, 5.53; N, 15.38. Found: C, 52.59; H, 5.67; N, 15.46.

5-(2-Fluorophenyl)-N'-(2,3,4,5,6-pentahydroxyhexylidene)–1H-pyrazole-3-carbohydrazide (**8b**).

White precipitates, Yield: 65%, mp 203–207 °C. IR (KBr, cm^{-1}): 3385, 2913, 1648, 1279. ^{1}HNMR (500 MHz, DMSO-d_6) (different isomers):13.65 (s, 1H, NH), 9.91 (bs, 1H, NHCO), 7.99–7.89 (m, 2 H, H4, H6), 7.78 (d, J = 6.3 Hz, 1H, CH = N), 7.41–7.23 (m, 6 H, 2 × H3, 2 × H5, 2 × pyrazole), 6.04–5.78 (m, 1H, OH), 5.61–5.48 (m, 1H, OH), 5.09–4.14 (m, 8 H, 8 × OH), 3.97–3.80 (m, 2 H, 2 × CH of Carbohydrate), 3.71–3.38 (m, 6 H, 6 × CH of Carbohydrate, partially overlapped with solvent), 3.27–3.22 (m, 1H, CH of Carbohydrate), 3.19–3.14 (m, 1H, CH of Carbohydrate), 3.07-3.00 (m, 2 H, 2 × CH of Carbohydrate) ppm. ^{13}CNMR (125 MHz, DMSO-d_6) (different isomers): 159.2 (d, J_{C-F} = 247.7 Hz), 159.1, 156.5, 152.9, 150.8, 130.5 (d, J_{C-F} = 6.3 Hz), 128.5, 125.3, 119.3, 116.8 (d, J_{C-F} = 22.5 Hz), 106.1, 106.0, 91.2, 88.5, 78.5, 77.5, 77.1, 74.1, 73.2, 72.4, 71.8, 71.6, 71.5, 71.4, 71.2, 70.8, 70.6, 63.9, 61.8, 61.1 ppm. Calcd for $C_{16}H_{19}FN_4O_6$: C, 50.26; H, 5.01; N, 14.65. Found: C, 50.13; H, 5.12; N, 14.76.

5-(2-Chlorophenyl)-N'-(2,3,4,5,6-pentahydroxyhexylidene)–1H-pyrazole-3-carbohydrazide (**8**c).

White precipitates, Yield: 70%, mp 168–172 °C. IR (KBr, cm^{-1}): 3371, 2924, 1649, 1280. ^{1}HNMR (500 MHz, DMSO-d_6) (different isomers): 13.80 (s, 1H, NH), 9.88 (bs, 1H, NHCO), 7.79–7.71 (m, 2 H, H3, H6), 7.57 (d, J = 7.4 Hz, 1H, CH = N), 7.45–7.36 (m, 3 H, H4, H5, pyrazole), 5.90 (bs, 1H, OH), 5.10–4.90 (m, 3 H, 3 × OH), 4.49–4.19 (m, 2 H, 2 × OH), 3.96–3.78 (m, 2 H, 2 × CH of Carbohydrate), 3.70–3.44 (m, 4 H, 4 × CH of Carbohydrate), 3.24–3.21 (m, 1H, CH of Carbohydrate), 3.16–3.13 (m, 1H, CH of Carbohydrate), 3.06–2.99 (m, 2 H, CH of Carbohydrate) ppm. ^{13}CNMR (125 MHz, DMSO-d_6) (different isomers): 160.9, 159.1, 156.1, 149.0, 131.5, 130.9, 130.8, 130.6, 130.4, 127.9, 106.7, 91.2, 88.4, 78.5, 77.1, 74.0, 72.4, 71.6, 70.8, 61.8, 61.3 ppm. Calcd for $C_{16}H_{19}ClN_4O_6$: C, 48.19; H, 4.80; N, 14.05. Found: C, 48.10; H, 4.97; N, 14.18.

5-(4-Fluorophenyl)-N'-(2,3,4,5,6-pentahydroxyhexylidene)–1H-pyrazole-3-carbohydrazide (**8d**).

White precipitates, Yield: 75%, mp 216–220 °C. IR (KBr, cm^{-1}): 3378, 2917, 1649, 1271. ^{1}HNMR (500 MHz, DMSO-d_6): 13.68 (s, 1H, NH), 9.67 (bs, 1H, NHCO), 7.85–7.83 (m, 3 H, CH = N, H2, H6), 7.30–7.28 (m, 3 H, H3, H5, pyrazole), 5.62–5.61 (m, 1H, OH), 5.49–5.46 (m, 1H, OH), 4.97–4.86 (m, 3 H, 3 × OH), 4.49–4.48 (m, 1H, CH of Carbohydrate), 4.30–4.28 (m, 1H, CH of Carbohydrate), 3.92–3.89 (m, 1H, CH of Carbohydrate), 3.68–3.65 (m, 1H, CH of Carbohydrate), 3.50–3.46 (m, 1H, CH of Carbohydrate), 3.17–3.14 (m, 1H, CH of Carbohydrate) ppm. ^{13}CNMR (125 MHz, DMSO-d_6) (different isomers): 162.2 (d, J_{C-F} = 298.5 Hz), 161.4, 158.7, 157.3, 146.8, 130.2, 127.8 (d, J_{C-F} = 9.3 Hz), 116.3 (d, J_{C-F} = 20.1 Hz), 103.3, 91.1, 88.5, 78.5, 77.2, 74.1, 72.4, 71.5, 70.6, 61.8, 61.4ppm. Calcd for $C_{16}H_{19}FN_4O_6$: C, 50.26; H, 5.01; N, 14.65. Found: C, 50.31; H, 5.17; N, 14.52.

5-(4-Chlorophenyl)-N'-(2,3,4,5,6-pentahydroxyhexylidene)–1H-pyrazole-3-carbohydrazide (**8e**).

White precipitates, Yield: 77%, mp 238–241 °C. IR (KBr, cm^{-1}): 3378, 2915, 1652, 1287. ^{1}HNMR (500 MHz, DMSO-d_6) (different isomers): 13.77–13.71 (m, 2 H, 2 ×NH), 10.09–10.08 (m, 1H, NHCO), 9.97–9.95 (m, 1H, NHCO), 9.66–9.65 (m, 1H, NHCO), 9.41–9.40 (m, 1H, NHCO), 7.86–7.73 (m, 6 H, 2 × CH = N, 2 × H2, 2 × H6), 7.54 (d, J = 7.9 Hz, 2 H, H3, H5), 7.48 (d, J = 7.9 Hz, 2 H, H3, H5), 7.35 (s, 1H, pyrazole), 7.24 (s, 1H, pyrazole), 7.16 (s, 1H, pyrazole), 7.12 (s, 1H, pyrazole), 5.96–5.72 (m, 1H, OH), 5.60–5.58 (m, 1H, OH), 5.49–5.46 (m, 1H, OH), 5.11–5.05 (m, 1H, OH), 4.97–4.91 (m, 1H, OH), 4.88–4.82 (m, 1H, CH of Carbohydrate), 4.52–4.24 (m, 2 H, 2 × CH of Carbohydrate), 3.93–3.86 (m, 1H, CH of Carbohydrate), 3.69–3.58 (m, 1H, CH of Carbohydrate), 3.49–3.43 (m, 1H, CH of Carbohydrate), 3.24–3.19 (m, 1H, CH of Carbohydrate), 3.15–3.11 (m, 1H, CH of Carbohydrate), 3.04–2.97 (m, 1H, CH of Carbohydrate) ppm. ^{13}CNMR (125 MHz, DMSO-d_6) (different isomers): 161.7, 159.1, 156.7, 152.2, 129.6, 129.3, 127.6, 127.2, 103.7, 91.3, 78.6, 77.1, 76.3, 74.1, 72.4, 71.5, 70.8, 70.7, 61.8 ppm. Calcd for $C_{16}H_{19}ClN_4O_6$: C, 48.19; H, 4.80; N, 14.05. Found: C, 48.06; H, 4.92; N, 14.17.

5-(4-Bromophenyl)-N'-(2,3,4,5,6-pentahydroxyhexylidene)–1H-pyrazole-3-carbohydrazide (**8f**).

White precipitates, Yield: 71%, mp > 250 °C. IR (KBr, cm^{-1}): 3369, 2911, 1644, 1273. ^{1}HNMR (500 MHz, DMSO-d_6): 13.77 (bs, 1H, NH), 9.69 (bs, 1H, NHCO), 7.80–7.57 (m, 5 H, CH = N, H2, H3, H5, H6), 7.20 (s, 1H, pyrazole), 5.97–5.49 (m, 1H, OH), 5.10–4.87 (m, 2 H, 2 × OH), 4.54–4.22 (m, 2 H, 2 × OH), 3.95–3.89 (m, 1H, CH of Carbohydrate), 3.70–3.65 (m, 1H, CH of Carbohydrate), 3.48–3.46 (m, 1H, CH of Carbohydrate), 3.25–3.22 (m, 1H, CH of Carbohydrate), 3.17–3.14 (m, 1H, CH of Carbohydrate), 3.05–2.99 (m, 1H, CH of Carbohydrate) ppm. ^{13}CNMR (125 MHz, DMSO-d_6) (different isomers): 161.6, 151.8, 150.1, 147.5, 132.4, 132.0, 127.7, 127.3, 103.5, 91.2, 88.5, 78.4, 77.1, 74.1, 72.4, 71.6, 71.5, 70.8, 61.8 ppm. Calcd for $C_{16}H_{19}BrN_4O_6$: C, 43.36; H, 4.32; N, 12.64. Found: C, 43.20; H, 4.47; N, 12.51.

5-(2,4-Dichlorophenyl)-N'-(2,3,4,5,6-pentahydroxyhexylidene)–1H-pyrazole-3-carbohydrazide (**8g**).

White precipitates, Yield: 65%, mp > 250 °C. IR (KBr, cm^{-1}): 3368, 2917, 1660, 1267. ^{1}HNMR (500 MHz, DMSO-d_6) (different isomers): 14.10 (s, 1H, NH), 9.87 (bs, 1H, NHCO), 7.83–7.66 (m, 3 H, CH = N, H3, H6), 7.55–7.38 (m, 2 H, H5, pyrazole), 5.88 (bs, 1H, OH), 5.61–5.50 (m, 1H, OH), 5.12–4.77 (m, 2 H, 2 × OH), 4.63–4.27 (m, 3 H, 3 × OH), 4.03–3.82 (m, 1H, CH of Carbohydrate), 3.71–3.44 (m, 2 H, 2 × CH of Carbohydrate), 3.25–2.89 (m, 3 H, 3 × CH of Carbohydrate) ppm. ^{13}CNMR (125 MHz, DMSO-d_6) (different isomers): 163.8, 159.1, 150.1, 147.6, 134.4, 133.4, 131.9, 130.2, 128.1, 127.3, 105.6, 97.4, 92.7, 91.2, 78.5, 77.2, 77.1, 77.0, 75.3, 74.0, 73.6, 72.8, 72.4, 72.3, 71.6, 71.1, 70.8, 70.7, 63.9, 61.8, 61.7 ppm. Calcd for $C_{16}H_{18}Cl_2N_4O_6$: C, 44.36; H, 4.19; N, 12.93. Found: C, 44.20; H, 4.08; N, 12.77.

5-(4-Nitrophenyl)-N'-(2,3,4,5,6-pentahydroxyhexylidene)–1H-pyrazole-3-carbohydrazide (**8h**).

White precipitates, Yield: 72%, mp 184–187 °C. IR (KBr, cm^{-1}): 3390, 2911, 1662, 1548, 1357, 1281. ^{1}HNMR (500 MHz, DMSO-d_6) (different isomers): 13.73 (bs, 1H, NH), 9.96 (bs, 1H, NHCO), 8.30 (d, J = 8.3 Hz, 2 H, H3, H5), 8.25 (d, J = 8.3 Hz, 2 H, H3, H5), 8.20–7.94 (m, 3 H, CH = N, H2, H6), 7.46 (s, 1H, pyrazole), 5.98–3.31 (m, 8 H, 5 × OH, 3 × CH of Carbohydrate, partially overlapped with solvent), 3.27–2.97 (m, 3 H, 3 × CH of Carbohydrate) ppm. ^{13}CNMR (125 MHz, DMSO-d_6) (different isomers): 160.3, 159.1, 153.2, 148.1, 147.2, 129.7, 126.5, 124.8, 104.5, 97.4, 92.8, 91.2, 88.5, 78.5, 77.2, 77.1, 75.3, 73.9, 73.5, 72.8, 72.4, 71.6, 70.8, 70.4, 63.8, 61.8, 61.7, 61.1 ppm. Calcd for $C_{16}H_{19}N_5O_8$: C, 46.95; H, 4.68; N, 17.11. Found: C, 46.82; H, 4.76; N, 17.19.

N'-(2,3,4,5,6-Pentahydroxyhexylidene)−5-(m-tolyl)−1H-pyrazole-3-carbohydrazide (**8i**).

White precipitates, Yield: 70%, mp 206–210 °C. IR (KBr, cm^{-1}): 3378, 2916, 1655, 1283. ^{1}HNMR (500 MHz, DMSO-d_6) (different isomers): 13.64 (s, 1H, NH), 9.65 (bs, 1H, NHCO), 7.66–7.56 (m, 3 H, CH=N, H2, H6), 7.35–7.32 (m, 1H, H5), 7.20–7.12 (m, 2 H, H4, pyrazole), 5.88 (bs, 1H, OH), 5.61–5.59 (m, 1H, OH), 5.48 (bs, 1H, OH), 5.09 (bs, 1H, OH), 4.95–4.85 (m, 2 H, 2 × OH), 4.52–4.18 (m, 3 H, 3 × CH of Carbohydrate), 3.93–3.87 (m, 1H, CH of Carbohydrate), 3.70–3.59 (m, 1H, CH of Carbohydrate), 3.48–3.44 (m, 1H, CH of Carbohydrate), 3.24–3.20 (m, 1H, CH of Carbohydrate), 3.16–3.13 (m, 1H, CH of Carbohydrate), 3.05–2.98 (m, 1H, CH of Carbohydrate), 2.35 (s, 3 H, CH$_3$) ppm. ^{13}CNMR (125 MHz, DMSO-d_6) (different isomers): 160.9, 159.1, 152.4, 148.3, 138.7, 129.3, 126.3, 122.9, 114.5, 110.1, 103.1, 91.1, 88.6, 78.5, 77.1, 74.1, 73.2, 72.4, 71.8, 71.5, 71.4, 71.2, 70.8, 63.9, 61.8, 21.5 ppm. Calcd for C$_{17}$H$_{22}$N$_4$O$_6$: C, 53.96; H, 5.86; N, 14.81. Found: C, 53.73; H, 5.62; N, 14.97.

N'-(2,3,4,5,6-Pentahydroxyhexylidene)−5-(p-tolyl)−1H-pyrazole-3-carbohydrazide (**8j**).

White precipitates, Yield: 68%, mp 232–236 °C. IR (KBr, cm^{-1}): 3386, 2921, 1662, 1269. ^{1}HNMR (500 MHz, DMSO-d_6): 13.58 (s, 1H, NH), 9.61 (bs, 1H, NHCO), 7.68–7.66 (m, 3 H, CH=N, H2, H6), 7.27–7.25 (m, 3 H, H3, H5, pyrazole), 5.60–5.58 (m, 1H, OH), 5.47 (bs, 1H, OH), 4.85–4.83 (m, 2 H, 2 × OH), 4.46 (bs, 1H, OH), 4.27–4.24 (m, 1H, CH of Carbohydrate), 3.89–3.87 (m, 1H, CH of Carbohydrate), 3.66–3.63 (m, 1H, CH of Carbohydrate), 3.47–3.44 (m, 2 H, 2 × CH of Carbohydrate), 3.14–3.12 (m, 1H, CH of Carbohydrate), 2.32 (s, 3 H, CH$_3$) ppm. ^{13}CNMR (125 MHz, DMSO-d_6): 164.7, 158.7, 156.2, 147.2, 130.9, 130.0, 127.8, 125.6, 102.7, 88.5, 74.1, 72.4, 71.5, 70.6, 61.3, 21.3 ppm. Calcd for C$_{17}$H$_{22}$N$_4$O$_6$: C, 53.96; H, 5.86; N, 14.81. Found: C, 53.81; H, 5.94; N, 14.69.

5-(3-Methoxyphenyl)-N'-(2,3,4,5,6-pentahydroxyhexylidene)−1H-pyrazole-3-carbohydrazide (**8k**).

White precipitates, Yield: 71%, mp 195–199 °C. IR (KBr, cm^{-1}): 3388, 2914, 1651, 1287, 1076. ^{1}HNMR (500 MHz, DMSO-d_6): 13.69 (bs, 1H, NH), 9.71 (bs, 1H, NHCO), 7.41–7.36 (m, 4 H, CH=N, H4, H5, H6), 7.15 (s, 1H, H2), 6.92 (s, 1H, pyrazole), 5.59–5.47 (m, 1H, OH), 5.08–4.85 (m, 1H, OH), 4.55–4.26 (m, 2 H, 2 × OH), 3.91–3.85 (m, 1H, OH), 3.81 (s, 3 H, OMe), 3.69–3.63 (m, 1H, CH of Carbohydrate), 3.53–3.37 (m, 3 H, 3 × CH of Carbohydrate), 3.21–2.97 (m, 2 H, 2 × CH of Carbohydrate) ppm. ^{13}CNMR (125 MHz, DMSO-d_6): 160.2, 155.8, 154.1, 149.3, 146.1, 131.0, 130.6, 121.8, 118.0, 114.6, 106.4, 88.5, 74.1, 72.4, 71.5, 70.6, 55.7 ppm. Calcd for C$_{17}$H$_{22}$N$_4$O$_7$: C, 51.77; H, 5.62; N, 14.21. Found: C, 51.65; H, 5.48; N, 14.39.

5-(4-Methoxyphenyl)-N'-(2,3,4,5,6-pentahydroxyhexylidene)−1H-pyrazole-3-carbohydrazide (**8l**).

White precipitates, Yield: 77%, mp 229–231 °C. IR (KBr, cm^{-1}): 3391, 2918, 1662, 1279, 1083. ^{1}HNMR (500 MHz, DMSO-d_6) (different isomers): 13.50 (bs, 1H, NH), 9.60 (bs, 1H, NHCO), 7.76–7.72 (m, 3 H, CH=N, H2, H6), 7.06–6.94 (m, 4 H, H3, H5, 2 × pyrazole), 5.86 (bs, 1H, OH), 5.60–5.47 (m, 2 H, 2 × OH), 5.23–4.48 (m, 4 H, 4 × OH), 4.58–4.19 (m, 4 H, 3 × OH, CH of Carbohydrate), 3.93–3.88 (m, 2 H, 2 × CH of Carbohydrate), 3.78 (s, 6 H, 2 × OMe), 3.70–3.59 (m, 3 H, 3 × CH of Carbohydrate), 3.51–3.44 (m, 3 H, 3× CH of Carbohydrate), 3.25–2.98 (m, 3 H, 3× CH of Carbohydrate) ppm. ^{13}CNMR (125 MHz, DMSO-d_6) (different isomers): 161.2, 159.5, 152.3, 146.9, 143.7, 127.3, 126.8, 121.8, 114.9, 114.7, 102.4, 91.1, 88.6, 77.0, 74.1, 72.4, 71.5, 70.7, 63.9, 61.8, 61.5, 55.7 ppm. Calcd for C$_{17}$H$_{22}$N$_4$O$_7$: C, 51.77; H, 5.62; N, 14.21. Found: C, 51.83; H, 5.50; N, 14.43.

5-(3,4-Dimethoxyphenyl)-N'-(2,3,4,5,6-pentahydroxyhexylidene)−1H-pyrazole-3-carbohydrazide (**8m**).

White precipitates, Yield: 75%, mp 173–177 °C. IR (KBr, cm^{-1}): 3376, 2910, 1657, 1293, 1089. ^{1}HNMR (500 MHz, DMSO-d_6): 13.58 (bs, 1H, NH), 9.65 (bs, 1H, NHCO), 7.38–7.33 (m, 3 H, CH=N, H2, H6), 7.14–7.02 (m, 2 H, H5, pyrazole), 5.88–5.60 (m, 1H, OH), 5.09–4.94 (m, 2 H, 2 × OH), 4.46–4.20 (m, 2 H, 2 × OH), 3.87–3.82 (m, 4 H, OMe, CH of Carbohydrate), 3.78–3.74 (m, 4 H, OMe, CH of Carbohydrate), 3.22–3.02 (m, 4 H, 4 × CH of Carbohydrate) ppm. ^{13}CNMR (125 MHz, DMSO-d_6) (different isomers): 159.2, 156.2, 152.5, 149.5, 144.1, 136.8, 131.0, 118.3, 112.5, 109.5, 102.7, 91.1, 88.6, 78.5, 77.1, 74.1, 73.1, 72.4, 71.8, 71.5, 71.2, 70.8, 63.9, 61.8, 61.4, 56.1, 56.0 ppm. Calcd for C$_{18}$H$_{24}$N$_4$O$_8$: C, 50.94; H, 5.70; N, 13.20. Found: C, 50.71; H, 5.53; N, 13.38.

Biological studies

In vitro α-glucosidase inhibitory study

α-Glucosidase (derived from *Saccharomyces cerevisiae*; EC3.2.1.20, 20 U/mg) and *p*-nitrophenyl α-D-glucopyranoside (*p*-NPG) were obtained Sigma-Aldrich. Potassium phosphate buffer (PPB, pH 6.8, 50 mM) and dimethyl sulfoxide (DMSO, final concentration of 10%) were used to prepare enzyme and test compounds solutions, respectively. Initially, the 96-well plate was filled with 20 μL of the test compounds, 20 μL of α-glucosidase (final concentration of 0.1 U/mL), and 135 μL of PPB. The mixture was then incubated at 37 °C for 10 min. Each well subsequently received 25 μL of the substrate (*p*-NPG, 4 mM), which was then incubated for 20 min at 37 °C. A Synergy HTX, (spectrophotometer, Bio-Tek, Germany), was used to measure the changes in the absorbance at 405 nm. Finally, the following formulas were used to determine the inhibitory percentages of the samples, positive control (acarbose), and negative control (DMSO):

$$[(Abs\ negative\ control\ -\ Abs\ sample)\ /Abs\ negative\ control]\ \times\ 100$$

A nonlinear regression curve of the compounds was used to determine the IC$_{50}$values[44].

Kinetic studies of α-glucosidase

When compound **8g** was present at various doses (0, 0.12, 0.25 and 0.5 μM) and *p*-NPG (2–10 mM) was used as the substrate, the manner of inhibition of the most active compound **8g** against α-glucosidase was examined. The Michaelis-Menten constant (K_m) was determined from the plot between the reciprocal of the substrate concentration (1/[S]) and the reciprocal of the enzyme rate (1/V) over a range of inhibitor concentrations. A Lineweaver-Burk plot was created to determine the type of inhibition. By creating secondary plots of the inhibitor concentration [I] vs. K_m, the experimental inhibitor constant (K_i) was determined.

Fluorescence spectroscopy measurements

Using a Synergy HTX multimode reader (Biotek Instruments, Winooski, VT, USA) fitted with a 1.0 cm quartz cell holder, the steady-state fluorescence emission spectra were recorded between 300 and 500 nm at an excitation wavelength of 280 nm. A 3.0 ml solution containing a fixed quantity of α-glucosidase was supplemented with compound **8g** at varying doses (ranging from 0 to 500 nM). Changes in hydrophobic patches can be analyzed in any folded/unfolded form of the enzyme. Before the measurements were taken, each mixture was allowed to equilibrate for ten minutes. The background fluorescence was obtained by subtracting the fluorescence spectra of the buffer without the enzyme[45].

Thermodynamic analysis of the binding of compound 8g to α-glucosidase

Hydrogen bonds, van der Waals forces, electrostatic attractions, and hydrophobic interactions are examples of non-covalent interactions that typically generate forces between ligands and proteins. To elucidate the binding forces within the complex of **8g** and α-glucosidase, the standard enthalpy change (ΔH°), standard entropy change (ΔS°), and standard free energy change (ΔG°)—the thermodynamic parameters of the noncovalent interactions—were determined in the following manner. To do this, the two-state equilibrium model N ↔ U was used to monitor the fluorescence intensity at 340 nm for various temperatures (298–338 K) to assess the stability of α-glucosidase in the presence or absence of **8g**. The fluorescence intensity data are displayed as a function of temperature and the thermodynamic profile was calculated via the techniques outlined in Mojtabavi et al.[46,47]. Consequently, using Eq. 1 and the assumption that protein denaturation occurs in two states, the denatured fraction (FD) of protein was computed.

$$F_D = \ (Y_N - Y_{obs}) / (Y_N - Y_D) \tag{1}$$

Y_N, Y_D and Y_{obs} are the values of the absorbance properties of a fully native and denatured conformation and the observed absorbance, respectively (Eq. 1)[46,47].

Furthermore, the apparent equilibrium constant (K) for a reversible denaturation process between the native and denatured protein states was determined via Eq. 2[46,47].

$$K = \ F_D / 1 - F_D = \ (Y_{obs} - Y_D) / (Y_N - Y_D) \tag{2}$$

Additionally, the Gibbs free energy (ΔG°) which is the most valuable standard of protein conformational stability in thermal denaturation, is provided by Eq. 3 (T and R are the absolute temperature and the universal gas constant, respectively):

$$\Delta G \ = G_D^\circ - G_N^\circ = \ -RT \ln K \tag{3}$$

On the other hand, to measure variations in a system's Gibbs energy as a function of temperature, the integrated Gibbs–Helmholtz equation was applied as follows (ΔC_p is the heat capacity of α-glucosidase denaturation: 11.6 kJ/mol K[48]:

$$\Delta G^\circ = \ \Delta H_m^\circ \left(1 - (T/T_m)\right) - \Delta C_p \left[(T_m - T) + T Ln \ (T/T_m)\right] \tag{4}$$

Tm is the temperature at which the protein is half-denatured during thermal denaturation. Additionally, the standard enthalpy and entropy of denaturation are ΔH°_m and ΔS°_m, respectively.

$$\Delta H = T_m \Delta S$$

In vivo hypoglycemic activity assay

For in vivo studies of the strongest compound **8g**, five male Wistar rats, aged 9–12 weeks, with an average weight of 200 g, were kept in a ventilated room with a 12-hour light/dark cycle at room temperature. The animals were randomly divided into three groups: test, positive and negative controls. Before the trial, the rats were given free access to food and drink, and were fasted for sixteen hours to complete an oral sucrose tolerance test. The test compound was given orally to the animals in the test group at three doses (2.5, 5 and 10 mg/kg); distilled water was given to the negative control group and acarbose (5 mg/kg) was given to the positive control group. All the rats were fed 7.5 g/kg sucrose after 30 min. Blood samples were then drawn from the tail vein at 0, 30, 45, 60, and 120 min, and a glucometer (Medisign MM1100) was used to measure the glucose level. The Research Ethics Committees of Laboratory Animals of Tehran University of Medical Sciences approved all animal experiments in this study (Approval ID: IR.TUMS.AEC.1400.045). Every experimental technique was carried out under the rules and regulations that applied.

Finally, one-way ANOVA was used to analyze the data[49–51].

Docking study

The homology model of the α-glucosidase structure used in this study was previously prepared by our research group[52]. First, non-essential components, such as water molecules, are removed from the enzyme. The structure of the ligand was drawn via ChemDraw. Ligand optimization was performed via Gaussian software. Autodock4 was used for docking. The grid box center (x = 81.609, y = 64.759, z = 38.92) was determined with a cubic box size of 60*60*60 via the Cα of key residues in the binding site of α-glucosidase. Docking studies were conducted utilizing the Lamarckian genetic algorithm and 100 runs.

MD simulations

Molecular dynamics simulations were conducted using Gromacs. Compound **8g** was specifically prepared for MD simulations. First, the standard force field was obtained using the antechamber package. The expected complex between the ligand and α-glucosidase was enclosed within a dodecahedral box. To maintain electroneutrality, Na$^+$ ions were introduced, and explicit TIP3P water model molecules were added to solvate the system. The molecular dynamics protocol included energy minimization performed with 50,000 cycles of steepest descent to eliminate any bad contacts or clashes. A 100 ps NVT ensemble using the velocity rescale algorithm was used, and the simulations were performed in the NPT ensemble (100 ps), which maintains a constant number of particles (N), pressure (P), and temperature (T) throughout the simulation. The production run was performed without any positional restraints for 100 ns. Gromacs tools were used to analyze MD trajectories.

Results and discussion
Chemistry

Figure 2 depicts the synthesis of the target compounds **8a-m**, which began with the reaction of diethyl oxalate (**1**) and several acetophenone derivatives (**2**). Next, compound **3** reacted with hydrazine hydrate (**4**) in refluxing ethanol to produce derivatives of ethyl 5-aryl-1*H*-pyrazole-3-carboxylate (**5**). The ester group was changed to the hydrazide moiety (**6**) by the reaction of the latter compound with hydrazine hydrate (**4**) in ethanol at room temperature. Ultimately, compound **8** was produced via the reaction of compound **6** with glucose (**7**) in dry ethanol and acetic acid (HOAc) as a catalyst, under reflux conditions for 24 h.

The structure of all derivatives was determined using IR and NMR spectroscopy. The signal at 1680 cm^{-1} in the IR spectrum confirmed the presence of the carbonyl group. Synthesised compounds' NMR spectra typically revealed distinct isomers, most likely as a result of the hydrazide moiety's restricted C-N bond rotation[53], which is influenced by the electronic nature of the substituents attached to the pyrazole moiety and steric hindrance. It is also important to determine the dominant product (**A** or **B**) in the structure of compound **8** (Fig. 2). The peak
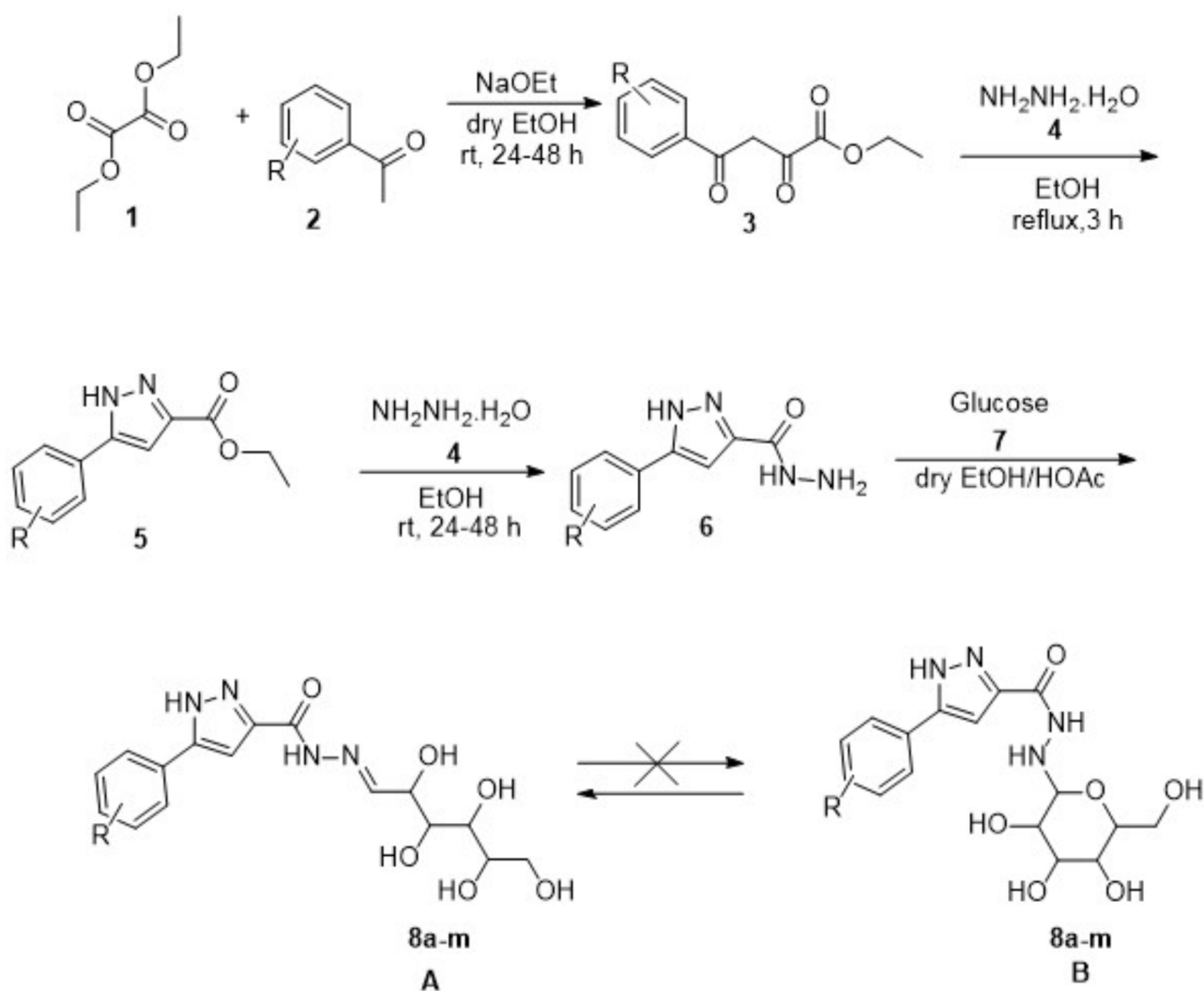
Fig. 2. Synthesis of pyrazole-glucose hybrids **8a-m**.

associated with the CH proton of N=CH was observed around 7.94–7.38 ppm in the ^{1}HNMR spectra, indicating that structure **A** was produced, whereas if compound **B** was obtained, this peak would not have been visible[34]. Notably, the peak around 5.97 and 4.19 ppm was associated with the OH groups of the sugar moiety, which were eliminated by the addition of D_2O. Additionally, the number of signals in the ^{13}CNMR spectra of the synthesized compounds matched the predicted number and chemical shifts.

Biological assay
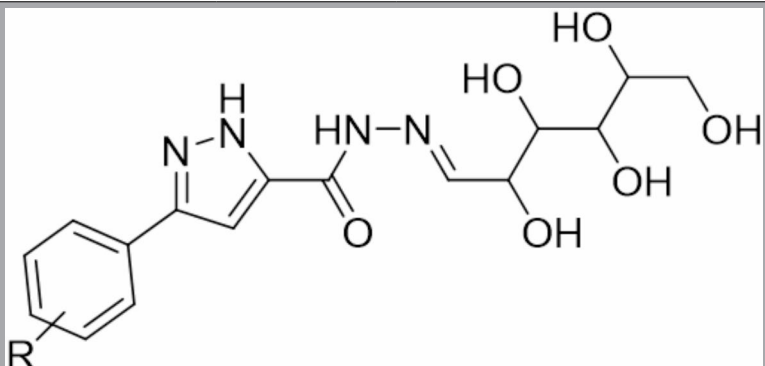
Enzyme inhibitory activity

The in vitro α-glucosidase inhibitory effects of all the synthesized 5-arylpyrazole-glucose hybrids (**8a-m**) were compared with acarbose as the positive control (Table 1). Compound **8a** lacking substituents on the aryl ring attached to the pyrazole moiety, showed substantial activity in the instance of α-glucosidase inhibitory activity when compared to acarbose ($IC_{50} = 1.2 \pm 0$ μM and 750.0 ± 5.0 μM, respectively).

Compounds **8k** and **8l** having methoxy groups at the *meta* or *para* positions of the aryl ring, depicted decreased inhibitory effects ($IC_{50} = 2.3 \pm 0$ μM), although their effects were still significantly greater than acarbose. Moreover, compound **8m** possessing more than one methoxy group, has the lowest level of effectiveness ($IC_{50} = 438.6 \pm 0.1$ μM). Additionally, compounds **8i** and **8j** with substituted a methyl group instead of the methoxy group, showed diminished activity ($IC_{50} = 12.1 \pm 0.5$ μM and 36.4 ± 0.2 μM, respectively). A moderate activiy was also shown by compound **8h**, which contained an electron withdrawing group (NO_2) ($IC_{50} = 80.5 \pm 0.7$ μM).

Compounds **8b** and **8d**, which contained fluorine at distinct locations on the aryl ring linked to the pyrazole moiety, exhibited lower efficiency than other halogenated derivatives (IC_{50} values of 53.9 ± 1.2 μM and 60.6 ± 1.0 μM, respectively). Placing chlorine in the *ortho* position slightly reduced the effectiveness (compound **8c**, $IC_{50} = 4.2 \pm 0.1$ μM) and placing it at the *para* position slightly increased the activity (compound **8e**, $IC_{50} = 1.0 \pm 0$ μM), however, with the simultaneous placement of two chlorine groups at the *ortho* and *para* positions, the inhibitor activity improved by approximately two times (compound **8g**, $IC_{50} = 0.5 \pm 0$ μM). Additionally, the effect decreased by the replacement of bromine at the *para* position (**8f**, $IC_{50} = 35.2 \pm 0.5$ μM).

Numerous studies have indicated that the sugar component can inhibit α-glucosidase, and computational studies have revealed potential hydrogen bonding interactions with important residues (Asp 518 and Asp 616) in the enzyme's active site[54–56]. Additionally, glycohybrids can improve pharmacological efficacy, decrease cytotoxicity, and enhance water solubility and bioavailability[36].

Compound 8	R	α-Glucosidase inhibition IC$_{50}$ (μM)[a]
8a	H	1.2 ± 0
8b	2-F	53.9 ± 1.2
8c	2-Cl	4.2 ± 0.1
8d	4-F	60.6 ± 1.0
8e	4-Cl	1.0 ± 0
8f	4-Br	35.2 ± 0.5
8g	2,4diCl	0.5 ± 0
8h	4-NO$_2$	80.5 ± 0.7
8i	3-Me	12.1 ± 0.5
8j	4-Me	36.4 ± 0.2
8k	3-OMe	2.3 ± 0
8l	4-OMe	2.3 ± 0
8m	3,4-diOMe	438.6 ± 0.1
Acarbose		750.0 ± 5.0

Table 1. Enzyme inhibitory activity of compound **8**. [a]Data are expressed as the mean ± SD (from three independent experiments)

Moreover, compounds including pyrazole-hydrazide (**B** and **E**, Fig. 1)[25,28] and glucose-hydrazide (**H**, Fig. 1)[34], demonstrated low to moderate inhibitory activity with IC_{50} values of 40.6, 60.5, and 292.2 µM, respectively, compared with acarbose, which has an IC_{50} of 750.0 µM. In comparison, these new hybrids show improved inhibitory effects with IC_{50} values ranging from 0.5 to 438.6 µM versus that of acarbose (IC_{50} = 750.0 µM). Thus, it appears that the hybridization of pyrazole, hydrazide, and glucose significantly enhances the inhibitory activity against α-glucosidase.

Kinetic studies

Compounds **8** was a potential candidate for kinetic analysis against α-glucosidase. As the concentration of the inhibitor increased, the Lineweaver-Burk plot (Fig. 3, a) revealed that the K_m steadily increased, but the V_{max} remained unchanged, suggesting that this chemical is a competitive inhibitor and is attached to the active site of the enzyme. Moreover, the inhibition constant K_i was estimated to be 0.46 µM on the basis of the plot of K_m against various inhibitor doses (Fig. 3, b).

Fluorescence spectroscopy measurements

Tryptophan, tyrosine, and phenylalanine in α-glucosidase cause the fluorescence properties; therefore, by examining the changes in the fluorescence intensity, it is possible to investigate changes in the structure of the enzyme in the presence of the inhibitor[39,57,58]. There are 18 tryptophan residues in α-glucosidase: 4 are located in the selected active site pocket (Trp381, Trp710, Trp715, and Trp789), and 8 are accessible to the surroundings. The interactions of compound **8g** with enzyme led to the alterations in the environment of tryptophan side chains [59]. Compound **8g** at the different concentrations (0–500 nM) did not show significant shift in the emission wavelength (λ_{max} 340 nm), but an increased intensity was observed. The shift in the fluorescence intensity indicated changes in the protein environment that resulted in structural unfolding and the subsequent exposure of tryptophan residues[46] (Fig. 4).

Thermodynamic analysis of the binding of compound 8g to α-glucosidase

Table 2 summarizes the values of $\Delta H°_m$ and $\Delta S°_m$. T_m. The calculated T_m was obtained as 304, 309 and 312 K in the presence of the inhibitor at 500, 250 and 125 nM, respectively. These findings showed that higher concentration of compound **8g** caused more instability (Fig. 5).

The sign of thermodynamic parameters categorized the forces between the ligand and protein into non-covalent interactions: hydrophobic interactions ($\Delta H° > 0$, $\Delta S° > 0$); van der Waals forces ($\Delta H° < 0$, $\Delta S° > 0$); hydrogen bondings and van der Waals interactions ($\Delta H° < 0$, $\Delta S° < 0$); and electrostatic interactions ($\Delta H° < 0$, $\Delta S° > 0$). Based on the results in Table 2, it seems that the addition of compound **8g** to aqueous solution of α-glucosidase strengthened the hydrophobic interactions, leading the protein to the unfolded state.

In vivo hypoglycemic effects

In vitro studies of compound **8g** showed a significant effect compared to other recent research. This hybrid was able to inhibit α-glucosidase 1500 times more potently than acarbose. For this reason, it seemed necessary to investigate its blood sugar-lowering effects, and in vivo study of compound **8g** was conducted in rats. For this purpose, sampling was performed via the tail vein at different times and the results of the subgraph area were analyzed via one-way ANOVA. The results showed that the inhibition and effectiveness of the compound at a dose of 2.5 mg/kg did not significantly differ from those of the negative control, but the effects of the compounds at the doses of 5 mg/kg and 10 mg/kg were significantly different (p-value < 0.05). On the other hand, the
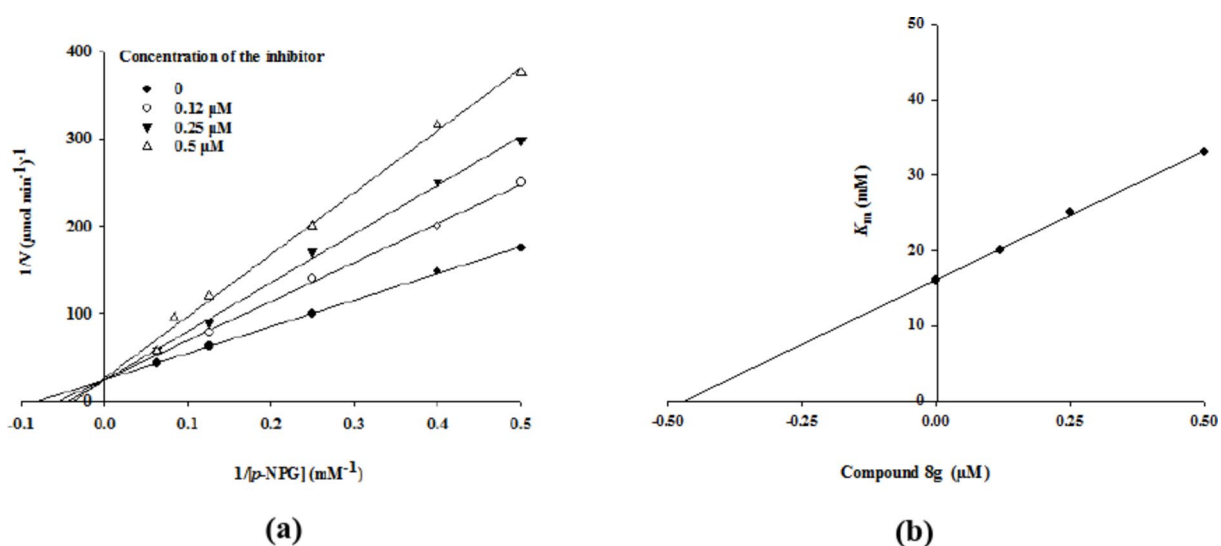

Fig. 3. (**a**) Line weaver-Burk plot of **8g** against α-glucosidase. (**b**) Double reciprocal Lineweaver-Burk plot of **8g** against α-glucosidase.

(a)

(b)
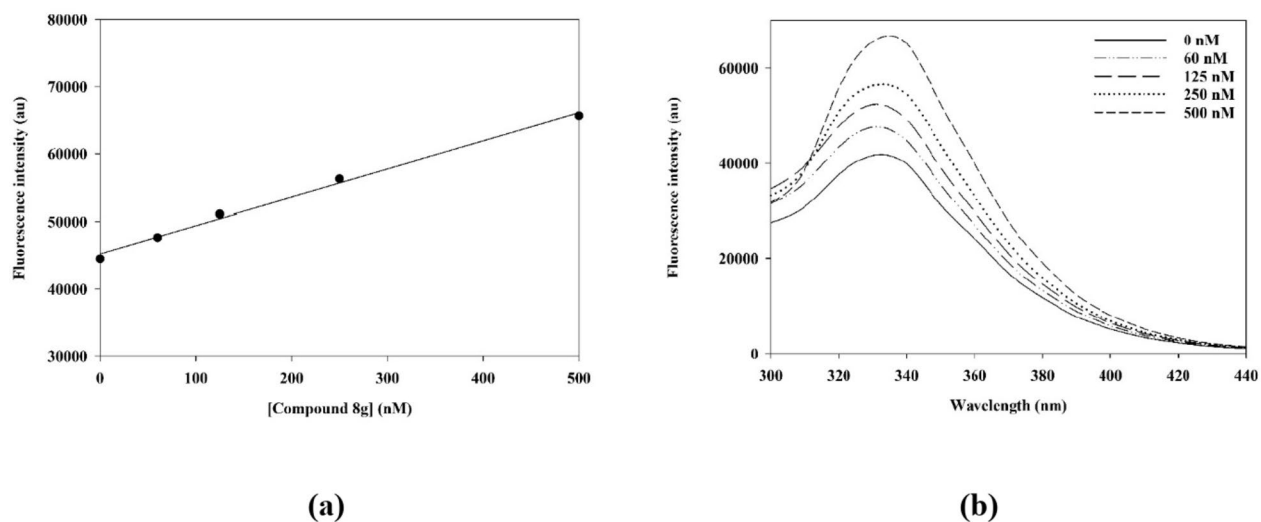
Fig. 4. (**a**) Fluorescence spectroscopy of α-glucosidase in the presence of compound **8g** at different concentrations (0–500 nM) in phosphate buffer (100 mM, pH 6.8). (**b**) Inset shows the changes in absorbance at 37 ℃ as a function of compound **8g.**

| Concentration of compound 8g (nM)	T_m (K)	ΔH_m° (kJ mol^{-1})	ΔS_m° (J mol^{-1} K^{-1})
0	317	5.7	18.2
60	314	103.2	328.6
125	312	132.8	425.6
250	309	144.3	466.9
500	304	157.1	516.4

Table 2. T_m, ΔH_m°, and ΔS_m° values for α-glucosidase at variable concentrations of compound **8 g**.
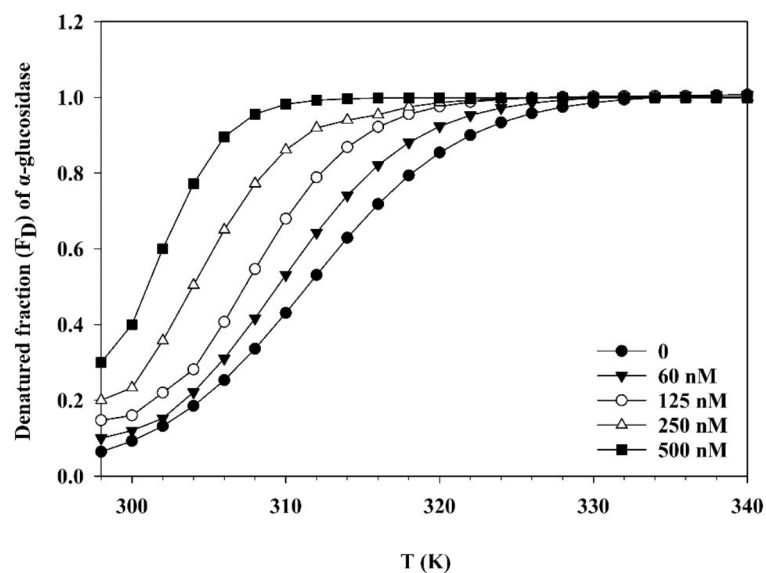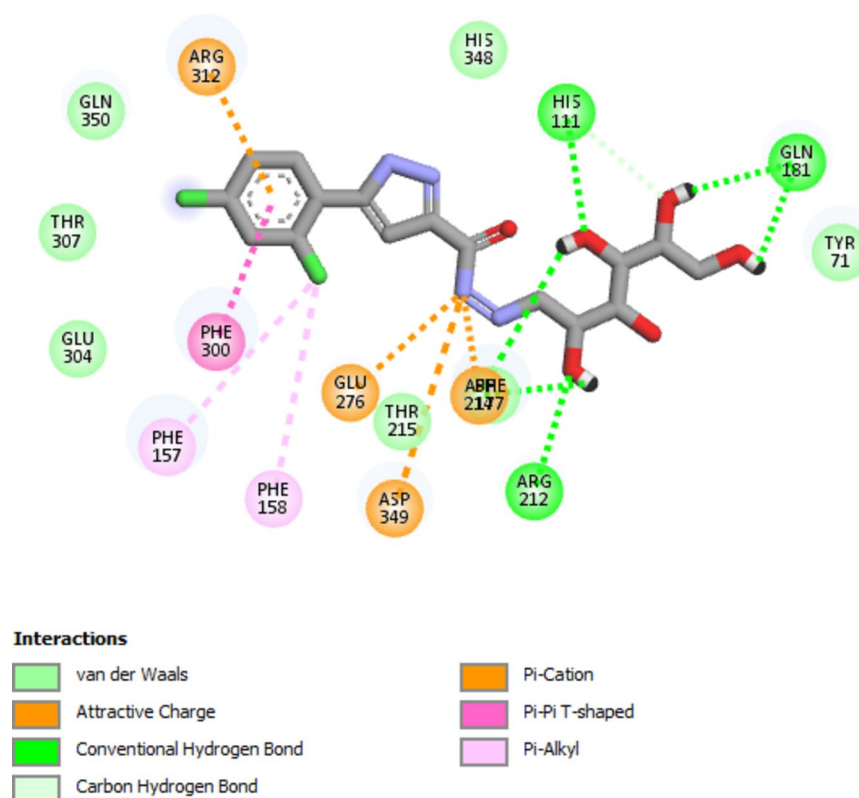

Fig. 5. Fraction of unfolded α-glucosidase in various concentrations of compound **8g** at pH 6.8.

effectiveness of these two prescription doses did not significantly differ from each other or from that of acarbose (5 mg/kg) Fig. 6).

Owing to the pharmacokinetic and pharmacodynamic effects, the results of the in vivo tests were not necessarily equivalent to those of the in vitro tests, as shown here.
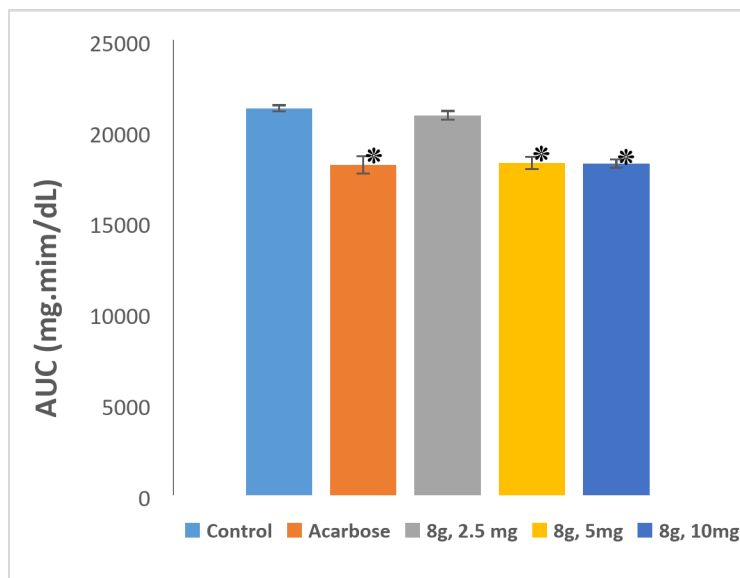
Fig. 6. The effects of acarbose and compound **8g** on normal rat glucose levels. Data were presented as the mean ± SD, *P < 0.05.

Interactions

▢	van der Waals	▢	Pi-Cation
▢	Attractive Charge	▢	Pi-Pi T-shaped
▢	Conventional Hydrogen Bond	▢	Pi-Alkyl
▢	Carbon Hydrogen Bond		

Fig. 7. The binding mode of compound **8g** to alpha-glucosidase active site.

Docking study

Compound **8g** with an IC$_{50}$ value of 0.5 µM, which was the most potent synthesized hybrid was selected for the molecular docking studies after kinetic and in vivo studies. Molecular docking studies of **8g** were performed using Autodock4. Compound **8g** exhibited a predicted free energy of binding of −6.01 kcal/mol when docked into the active site of α-glucosidase. The key amino acids in the active site of the α-glucosidase include Phe157, Arg212, Glu276, and Asp349. In Fig. 7, the predicted binding pose and interactions of compound **8g** with the
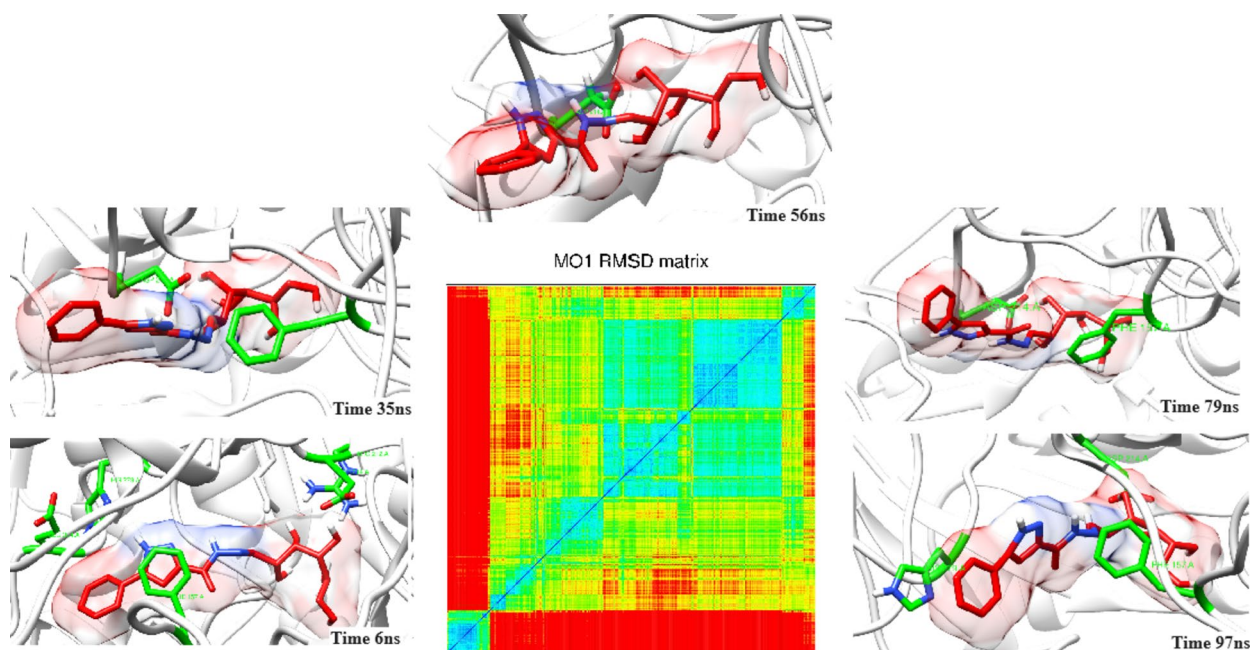
Fig. 8. RMSD matrix and trajectories of compound **8g** in the binding site of α-glucosidase during 100 ns of MD simulation. The red stick represents the ligand. Essential amino acids are shown as green sticks.

active site of enzyme are illustrated. At the *ortho* position of the benzyl ring in ligand **8g**, the Cl group interacted with residue Phe157 through a π-alkyl. The amino acid backbones Asp214, Glu276, and Asp349 ions interacted with the amide nitrogen. The hydroxyl group of the ligand interacted with the Arg212 residue through a hydrogen bonding interaction. Additionally, residues His111 and Gln181 formed hydrogen bonding interactions with the hydroxyl group of the ligand. Phe300 interacted with the benzyl moiety through π-π T-shaped interaction. A π-cation interaction was formed between the Arg312 residue and the benzyl moiety. Therefore, the results of both kinetic and molecular docking studies confirmed that compound **8g** interacted with the active site of the enzyme and effectively inhibited α-glucosidase in a competitive manner.

Molecular dynamic simulation

A 100 ns molecular dynamics simulation was performed in explicit water. The stability of the predicted **8g**-α-glucosidase complex in the docking phase was assessed through 100 ns MD simulations. The density of the simulated system was similar to the experimental results ($1024.11 \pm RSD = 0.19\%$), indicating that the applied force field could replicate the experimental results. The system's stability was assessed by observing thermodynamic variables, including temperature and total energy. The temperature ($RSD = 0.39\%$ K) and energy ($RSD = 0.18\%$) were stable during the simulation, and energy preservation was satisfactory. The average RMSD value for the complex was 0.927. Overall, the complex remained stable during the 100 ns MD simulation.

To evaluate the conformational changes of compound **8g** in the binding site of α-glucosidase, we assessed the RMSD matrix of the ligand and the trajectories of various transition times (red region in the RMSD matrix in Fig. 8). In the molecular dynamics study, from 6 ns to 35 ns, the sugar moiety maintained its position.

In contrast, the pyrazole moiety and the attached benzene ring moved upward, approaching a small alpha helix consisting of residues Pro240-Gly243. This movement expanded the active site pocket as the alpha helix shifted to accommodate the ligand's movement. Following this adjustment, the ligand stabilized in its new position until 79 ns. At 97 ns, while the sugar moiety remained stable, the pyrazole moiety and the aryl ring moved downward, wading away from the Pro240-Gly243 alpha helix.

At 6 ns the hydrogen bonding interction between the ligand and the enzyme played an important role. The hydroxyl portion of the sugar section made a key interaction with the Asp214 and Glu276 residues. Additionally, the pyrazole ring formed a key pi-pi stacking interaction with Phe157. Throughout the simulation, hydrogen bonding interactions were formed between the ligand and Asp214. By 56 ns, the pyrazole ring segment formed pi-alkyl interactions with the Ala278 and Leu218 residues. During molecular dynamics, a hydrogen bonding interaction between Gln181 and the sugar hydroxyl group was also established.

Conclusion

In this study, 13 different derivatives of novel 5-aryl pyrazole-glucose hybrids were designed and synthesized. These compounds showed significant inhibitory effects with IC_{50} values ranging from 0.5 to 438.6 μM compared to acarbose as a reference drug ($IC_{50} = 750.0$ μM). The analysis of the structure-activity relationship suggested that a lack of substitutions on the aryl ring, or the presence of chlorine or methoxy groups, can improve their effectiveness ($IC_{50} = 0.5$ to 4.2 μM). Furthermore, kinetic and molecular docking studies indicated that these compounds function as competitive inhibitors. Among them, compound **8g** containing two chlorine groups,

was recognized as the most effective inhibitor in this class (IC$_{50}$ = 0.5 μM) and was capable of lowering blood sugar levels in the rats at a dose similar to that of acarbose. Thus, continued investigation into these hybrids could lead to the discovery of more potent compounds for the management of type 2 diabetes.

Data availability

This published article and its supplementary information files include all data generated or analyzed during this study.

References

1. Sun, H. et al. IDF Diabetes Atlas: Global, regional and country-level diabetes prevalence estimates for 2021 and projections for 2045. *DRCP*. 183, 109119. (2022). https://doi.org/10.1016/j.diabres.2021.109119
2. Alam, S. et al. Diabetes mellitus: insights from epidemiology, biochemistry, risk factors, diagnosis, complications and comprehensive management. *Diabetology* 2, 36–50. https://doi.org/10.3390/diabetology2020004 (2021).
3. Tomic, D., Shaw, J. E. & Magliano, D. J. The burden and risks of emerging complications of diabetes mellitus. *Nat. Rev. Endocrinol.* 18, 525–539. https://doi.org/10.1038/s41574-022-00690-7 (2022).
4. Cloete, L. Diabetes mellitus: an overview of the types, symptoms, complications and management. *Nurs. Standard (Royal Coll. Nurs. (Great Britain): 1987).* https://doi.org/10.7748/ns.2021.e11709 (2021).
5. Padhi, S., Nayak, A. K. & Behera, A. Type II diabetes mellitus: A review on recent drug based therapeutics. *Biomed. Pharmacother.* 131, 110708. https://doi.org/10.1016/j.biopha.2020.110708 (2020).
6. Su, J., Luo, Y., Hu, S., Tang, L. & Ouyang, S. Advances in research on type 2 diabetes mellitus targets and therapeutic agents. *Int. J. Mol. Sci.* 24, 13381. https://doi.org/10.3390/ijms241713381 (2023).
7. Blahova, J. et al. Pharmaceutical drugs and natural therapeutic products for the treatment of type 2 diabetes mellitus. *Pharmaceuticals* 14, 806. https://doi.org/10.3390/ph14080806 (2021).
8. Hossain, U., Das, A. K., Ghosh, S. & Sil, P. C. An overview on the role of bioactive α-glucosidase inhibitors in ameliorating diabetic complications. *FCT* 145, 111738. https://doi.org/10.1016/j.fct.2020.111738 (2020).
9. Alssema, M. et al. Effects of alpha-glucosidase-inhibiting drugs on acute postprandial glucose and insulin responses: a systematic review and meta-analysis. *Nutr. Diabetes.* 11, 1–9. https://doi.org/10.1038/s41387-021-00152-5 (2021).
10. Pan, G. et al. A review on the in vitro and in vivo screening of α-glucosidase inhibitors. *Heliyon* 10, 37467. https://doi.org/10.1016/j.heliyon.2024.e37467 (2024).
11. Khan, F., Khan, M. V., Kumar, A. & Akhtar, S. Recent advances in the development of Alpha-Glucosidase and Alpha-Amylase inhibitors in type 2 diabetes management: insights from in Silico to in vitro studies. *Curr. Drug Targets.* 25, 782–795. https://doi.org/10.2174/0113894501313365240722100902 (2024).
12. Hedrington, M. S. & Davis, S. N. Considerations when using alpha-glucosidase inhibitors in the treatment of type 2 diabetes. *Expert Opin. Pharmaco.* 20, 2229–2235. https://doi.org/10.1080/14656566.2019.1672660 (2019).
13. Agrawal, N., Sharma, M., Singh, S. & Goyal, A. Recent advances of α-glucosidase inhibitors: A comprehensive review. *Curr. Top. Med. Chem.* 22, 2069–2086. https://doi.org/10.2174/1568026622666220831092855 (2022).
14. Mushtaq, A., Azam, U., Mehreen, S. & Naseer, M. M. Synthetic α-glucosidase inhibitors as promising anti-diabetic agents: recent developments and future challenges. *Eur. J. Med. Chem.* 249, 115119. https://doi.org/10.1016/j.ejmech.2023.115119 (2023).
15. Liu, S. K. et al. Discovery of new α-glucosidase inhibitors: Structure-based virtual screening and biological evaluation. *Front. Chem.* 9, 639279. https://doi.org/10.3389/fchem.2021.639279 (2021).
16. Singh, A. et al. Recent developments in synthetic α-glucosidase inhibitors: A comprehensive review with structural and molecular insight. *J. Mol. Struct.* 1281, 135115. https://doi.org/10.1016/j.molstruc.2023.135115 (2023).
17. Dhameja, M. & Gupta, P. Synthetic heterocyclic candidates as promising α-glucosidase inhibitors: an overview. *Eur. J. Med. Chem.* https://doi.org/10.1016/j.ejmech.2019.04.025 (2019). 343–77.
18. Patel, P. et al. A review on the development of novel heterocycles as α-Glucosidase inhibitors for the treatment of Type-2 diabetes mellitus. *Med. Chem.* 20, 503–536. https://doi.org/10.2174/0115734064264591231031065639 (2024).
19. Fallah, Z. et al. A review on synthesis, mechanism of action, and structure-activity relationships of 1, 2, 3-triazole-based α-glucosidase inhibitors as promising anti-diabetic agents. *J. Mol. Struct.* 1255, 132469. https://doi.org/10.1016/j.molstruc.2022.132469 (2022).
20. Ullah, H., Aslam, M. W., Rahim, F., Hussain, A. & Perviaz, M. Synthesis, in vitro α-glucosidase and α-amylase activities and molecular Docking study of oxadiazole-sulphonamide hybrid analogues. *Chem. Data Coll.* 45, 101031. https://doi.org/10.1016/j.cdc.2023.101031 (2023).
21. Li, Y. et al. Discovery of new 2-phenyl-1H-benzo [d] imidazole core-based potent α-glucosidase inhibitors: synthesis, kinetic study, molecular docking, and in vivo anti-hyperglycemic evaluation. *Bioinorg. Chem.* 117, 105423. https://doi.org/10.1016/j.bioorg.2021.105423 (2021).
22. Ullah, H. et al. Synthesis, in vitro α-glucosidase activity and in Silico molecular Docking study of Isatin analogues. *Chem. Data Coll.* 43, 100987. https://doi.org/10.1016/j.cdc.2022.100987 (2023).
23. Firdaus, J., Siddiqui, N., Alam, O., Manaithiya, A. & Chandra, K. Pyrazole scaffold-based derivatives: A glimpse of α-glucosidase inhibitory activity, SAR, and route of synthesis. *Arch. Pharm.* 356, 2200421. https://doi.org/10.1002/ardp.202200421 (2023).
24. Dhouib, I., Messaad, M., HadjKacem, B., Fendri, I. & Khemakhem, B. Pyrazole and pyrazolone derivatives as specific α-glucosidase inhibitors: in vitro combined with in Silico, hemolytic and cytotoxicity studies. *J. Mol. Struct.* 1294, 136331. https://doi.org/10.1016/j.molstruc.2023.136331 (2023).
25. Azimi, F. et al. Design, synthesis, biological evaluation, and molecular modeling studies of pyrazole-benzofuran hybrids as new α-glucosidase inhibitor. *Sci. Rep.* 11, 20776. https://doi.org/10.1038/s41598-021-99899-1 (2021).
26. Karrouchi, K. et al. Synthesis, crystal structure, DFT, α-glucosidase and α-amylase Inhibition and molecular Docking studies of (E)-N'-(4-chlorobenzylidene)-5-phenyl-1H-pyrazole-3-carbohydrazide. *J. Mol. Struct.* 1245, 131067. https://doi.org/10.1016/j.molstruc.2021.131067 (2021).
27. Kaur, R., Palta, K. & Kumar, M. Hybrids of Isatin-Pyrazole as potential α-Glucosidase inhibitors: synthesis, biological evaluations and molecular Docking studies. *ChemistrySelect* 4, 13219–13227. https://doi.org/10.1002/slct.201903418 (2019).
28. Azimi, F. et al. Design and synthesis of novel quinazolinone-pyrazole derivatives as potential α-glucosidase inhibitors: Structure-activity relationship, molecular modeling and kinetic study. *Bioorg. Chem.* 114, 105127. https://doi.org/10.1016/j.bioorg.2021.105127 (2021).
29. Mishra, S. et al. Carbohydrate-based therapeutics: a frontier in drug discovery and development. *Stud. Nat. Prod. Chem.* 49, 307–361. https://doi.org/10.1016/B978-0-444-63601-0.00010-7 (2016).
30. Kumari, P., Narayana, C., Tiwari, G. & Sagar, R. Glycohybrid molecules in medicinal chemistry: Present status and future prospective. *Carbohydrates in Drug Discovery and Development: Elsevier.* 451–79. (2020). https://doi.org/10.1016/B978-0-12-816675-8.00011-7

31. Cao, X. et al. Carbohydrate-based drugs launched during 2000–2021. *APSB* **12**, 3783–3821. https://doi.org/10.1016/j.apsb.2022.05.020 (2022).

32. Dirir, A. M., Daou, M., Yousef, A. F. & Yousef, L. F. A review of alpha-glucosidase inhibitors from plants as potential candidates for the treatment of type-2 diabetes. *Phytochem Rev.* **21**, 1049–1079. https://doi.org/10.1007/s11101-021-09773-1 (2022).

33. Gupta, S. J., Dutta, S., Gajbhiye, R. L., Jaisankar, P. & Sen, A. K. Synthesis, in vitro evaluation and molecular Docking studies of novel amide linked Triazolyl glycoconjugates as new inhibitors of α-glucosidase. *Bioinorg. Chem.* **72**, 11–20. https://doi.org/10.1016/j.bioorg.2017.03.006 (2017).

34. Hariri, R. et al. Synthesis of new Glucose-containing 5-Arylisoxazoles and their enzyme inhibitory activity. *Lett. Org. Chem.* **21**, 707–719. https://doi.org/10.2174/0115701786283334231228104931 (2024).

35. Zhang, Z-P. et al. Novel carbohydrate-triazole derivatives as potential α-glucosidase inhibitors. *CJNM* **18**, 729–737. https://doi.org/10.1016/S1875-5364(20)60013-9 (2020).

36. Mishra, V. K., Khanna, A., Tiwari, G., Tyagi, R. & Sagar, R. Recent developments on the synthesis of biologically active glycohybrids. *Bioorg. Chem.* **145**, 107172. https://doi.org/10.1016/j.bioorg.2024.107172 (2024).

37. Khan, H. et al. Design, synthesis, molecular Docking study, and α-glucosidase inhibitory evaluation of novel hydrazide–hydrazone derivatives of 3, 4-dihydroxyphenylacetic acid. *Sci. Rep.* **14**, 11410. https://doi.org/10.1038/s41598-024-62034-x (2024).

38. Islam, W. U. et al. Synthesis of novel Hydrazide schiff bases with anti-diabetic and anti-hyperlipidemic effects: in-vitro, in-vivo and in-silico approaches. *J. Biomol. Struct. Dyn.* https://doi.org/10.1080/07391102.2024.2329296 (2024).

39. Saeedi, M. et al. Novel N′-substituted benzylidene benzohydrazides linked to 1, 2, 3-triazoles: potent α-glucosidase inhibitors. *Sci. Rep.* **13**, 8960. https://doi.org/10.1038/s41598-023-36046-y (2023).

40. Saeedi, M. et al. Design and synthesis of novel arylisoxazole-chromenone carboxamides: investigation of biological activities associated with Alzheimer's disease. *Chem. Biodivers.* **17**, 1900746. https://doi.org/10.1002/cbdv.201900746 (2020).

41. Akbarzadeh, T. et al. 2-Amino-3-cyano-4-(5-arylisoxazol-3-yl)-4H-chromenes: synthesis and in vitro cytotoxic activity. *Arch. Pharm.* **345**, 386–392. https://doi.org/10.1002/ardp.201100345 (2012).

42. Ershov, A. Y., Martynenkov, A., Lagoda, I. & Yakimansky, A. Synthesis of Mono-and disaccharide 4-[(ω-Sulfanylalkyl) Oxy] benzoylhydrazones as potential glycoligands for noble metal nanoparticles. *Russ J. Gen. Chem.* **89**, 292–299. https://doi.org/10.1134/S1070363219020208 (2019).

43. Khalifa, N., Al-Omar, M. & Nossier, E. Antimicrobial activity of some new N-glycosylidene carbohydrazide derivatives. *Russ J. Gen. Chem.* **87**, 2909–2914. https://doi.org/10.1134/S1070363217120301 (2017).

44. Shareghi-Boroujeni, D. et al. Synthesis, in vitro evaluation, and molecular Docking studies of novel Hydrazineylideneindolinone linked to phenoxymethyl-1, 2, 3-triazole derivatives as potential α-glucosidase inhibitors. *Bioinorg. Chem.* **111**, 104869. https://doi.org/10.1016/j.bioorg.2021.104869 (2021).

45. Barker, M. K. & Rose, D. R. Specificity of processing α-glucosidase I is guided by the substrate conformation: crystallographic and in Silico studies. *JBC* **288**, 13563–13574. https://doi.org/10.1074/jbc.M113.460436 (2013).

46. Mojtabavi, S., Jafari, M., Samadi, N., Mehrnejad, F. & Faramarzi, M. A. Insights into the Molecular-Level details of betaine interactions with laccase under various thermal conditions. *J. Mol. Liq.* **339**, 116832. https://doi.org/10.1016/j.molliq.2021.116832 (2021).

47. Farhadian, S. et al. Insights into the molecular interaction between sucrose and α-chymotrypsin. *Int. J. Biol. Macromol.* **114**, 950–960. https://doi.org/10.1016/j.ijbiomac.2018.03.143 (2018).

48. Van Der Kamp, M. W. et al. Dynamical origins of heat capacity changes in enzyme-catalysed reactions. *Nat. Commun.* **9**, 1177. https://doi.org/10.1038/s41467-018-03597-y (2018).

49. Xie, H-X. et al. Novel tetrahydrobenzo [b] thiophen-2-yl) Urea derivatives as novel α-glucosidase inhibitors: synthesis, kinetics study, molecular docking, and in vivo anti-hyperglycemic evaluation. *Bioinorg. Chem.* **115**, 105236. https://doi.org/10.1016/j.bioorg.2021.105236 (2021).

50. Ruiz-Vargas, J. A. et al. α-Glucosidase inhibitory activity and in vivo antihyperglycemic effect of secondary metabolites from the leaf infusion of Ocimum campechianum mill. *J. Ethnopharmacol.* **243**, 112081. https://doi.org/10.1016/j.jep.2019.112081 (2019).

51. Yu, X. et al. Exploring efficacy of natural-derived acetylphenol scaffold inhibitors for α-glucosidase: synthesis, in vitro and in vivo biochemical studies. *BMCL* **30**, 127528. https://doi.org/10.1016/j.bmcl.2020.127528 (2020).

52. Ghorbani, H. et al. Synthesis, in vitro α-glucosidase inhibitory activity and molecular dynamics simulation of some new coumarin-fused 4H-pyran derivatives as potential anti-diabetic agents. *J. Mol. Struct.* **1284**, 135349. https://doi.org/10.1016/j.molstruc.2023.135349 (2023).

53. Iraji, A. et al. Cyanoacetohydrazide linked to 1, 2, 3-triazole derivatives: A new class of α-glucosidase inhibitors. *Sci. Rep.* **12**, 8647. https://doi.org/10.1038/s41598-022-11771-y (2022).

54. Ali, A., Cottrell, J. J., Dunshea, F. R. & Antioxidant alpha-glucosidase inhibition activities, in silico molecular docking and pharmacokinetics study of phenolic compounds from native Australian fruits and spices. *Antioxidants*. 12, 254. (2023). https://doi.org/10.3390/antiox12020254

55. Adinortey, C. A. et al. Molecular structure-based screening of the constituents of Calotropis procera identifies potential inhibitors of diabetes mellitus target alpha glucosidase. *CIMB* **44**, 963–987. https://doi.org/10.3390/cimb44020064 (2022).

56. Ali, A., Cottrell, J. J. & Dunshea, F. R. Identification and characterization of anthocyanins and non-anthocyanin phenolics from Australian native fruits and their antioxidant, antidiabetic, and anti-Alzheimer potential. *Int. Food Res. J.* **162**, 111951. https://doi.org/10.1016/j.foodres.2022.111951 (2022).

57. Yin, Y. et al. Mechanism of interaction between urolithin A and α-glucosidase: analysis by Inhibition kinetics, fluorescence spectroscopy, isothermal Titration calorimetry and molecular Docking. *J. Mol. Struct.* **1286**, 135567. https://doi.org/10.1016/j.molstruc.2023.135567 (2023).

58. Albrecht, C., Joseph, R. & Lakowicz *Principles of Fluorescence Spectroscopy* (Springer, 2008).

59. Jafari, M. et al. Molecular level insight into stability, activity, and structure of laccase in aqueous ionic liquid and organic solvents: an experimental and computational research. *J. Mol. Liq.* **317**, 113925. https://doi.org/10.1016/j.molliq.2020.113925 (2020).

Acknowledgements

Author contributions

RH collaborated on the synthesis and characterization of compounds, performed in vivo assay and wrote the manuscript. MS designed the project and wrote the manuscript. SM performed the α-glucosidase inhibition and the fluorometric assay. SA conducted a docking study and molecular dynamics calculation. AE supervised docking study and molecular dynamics calculations. MAF supervised biological assays. MA collaborated on the characterization of compounds. MSH supervised in vivo tests. MB and TA supervised all phases of the project.

Declarations

Competing interests
The authors declare no competing interests.

Additional information
Supplementary Information The online version contains supplementary material available at https://doi.org/10.1038/s41598-025-92706-1.

Correspondence and requests for materials should be addressed to T.A.

Reprints and permissions information is available at www.nature.com/reprints.

Publisher's note Springer Nature remains neutral with regard to jurisdictional claims in published maps and institutional affiliations.